Geomechanics and Engineering, *Vol. 28, No. 4 (2022) 405-419*
https://doi.org/10.12989/gae.2022.28.4.405

Analysis of cavity expansion and contraction in unsaturated residual soils

Alpha Lukose[a] and Sudheesh Thiyyakkandi*

Department of Civil Engineering, Indian Institute of Technology, Palakkad, Kerala, India

(Received June 4, 2021, Revised November 17, 2021, Accepted November 18, 2021)

Abstract. Cavity expansion and contraction solutions for cylindrical and spherical cavities in unsaturated residual soils are presented in this paper. Varying soil state in the plastic zone is accounted by a numerical approach, wherein an element-by-element discretization of the plastic zone of both expanding and contracting cavities is carried out. Unlike existing methods utilizing self-similarity technique, the solution procedure enables the prediction of entire soil-state at any stage of expansion and subsequent contraction. It is also applicable for both cavity creation and expansion problems. The approach adopts constant contribution of suction to effective stress (constant χs drainage condition) for analysis. The analysis procedure is validated by interpreting the previously reported pressuremeter test results in lateritic residual soil. The typical cavity expansion and contraction characteristics of unsaturated Indian lateritic soil were then examined using this solution procedure. The effect of initial soil-state on cavity limit pressure, plastic radius, reverse yield pressure, and reverse plastic radius are also presented.

Keywords: cavity contraction; cavity expansion; soil state; suction; unsaturated residual soil

1. Introduction

Residual soils are in-situ soils formed by chemical weathering and thus vary from kaolinitic lateritic soils and gravels to allophanic soils to the montmorillonitic black soils. The procurement of undisturbed samples of the residual soils, especially lateritic soils, for various laboratory testing is difficult due to their heterogeneity and high sensitivity to sampling processes. Since the laboratory testing of such lateritic/residual soil samples may not yield the true shear strength and stiffness characteristics of natural soil, in-situ tests such as cone penetration test, dilatometer and pressuremeter test (PMT) are vital (Schnaid *et al*. 2000); the results of which can be used to back-calculate the strength parameters and stiffness of soil. Back-computation of in-situ soil properties from the field test data (e.g., pressuremeter test) using cavity expansion and contraction theories were found to give relatively good results (Schnaid *et al*. 2000, Rouainia *et al.* 2020). In case of an in-situ test in unsaturated soil (i.e., above water table), the matric suction may have major influence on the observed strength and deformation responses. Therefore, stiffness and strength parameters obtained from interpretation of the in-situ test may yield erroneous results if the effect of suction is not accounted properly (Schnaid *et al.* 2000, Russell and Khalili 2006, Yang and Russell 2015b, Cheng *et al.* 2018).

The application of cavity expansion theory on saturated soil - drained (Li and Zou 2019, Li *et al.* 2019b) or undrained state (Li *et al.* 2020) - and dry soil (drained state) has gained large popularity in the last five decades and solutions for such problems have been proposed by several researchers. These include closed form solutions (Carter *et al.* 1986, Yu and Houlsby 1991, Yu and Carter 2002, Zhao *et al.* 2018, Li and Zou 2019a); semi-analytical solutions using the similarity technique (Collins *et al.* 1992, Collins and Stimpson 1994, Wang *et al.* 2021); and the numerical solutions (Salgado and Randolph 2001, Cao *et al.* 2002).

It is evident from literature that only very limited number of studies have been reported on cavity expansion analysis in unsaturated soils (Schnaid *et al.* 2004, Russell and Khalili 2006, Khalili *et al.* 2008, Yang and Russell 2015a, b, Cheng *et al.* 2018, Tang *et al.* 2021). For instance, Schnaid *et al.* (2004) used the closed form solutions proposed by Yu and Houlsby (1991) for the interpretation of suction monitored pressuremeter data in unsaturated residual granite soil. Though this method accounts for soil dilation and large strain effects, including elastic strain in the plastic zone, it cannot incorporate the variability of friction and dilation angles during the expansion process. Yang and Russell (2015a) extended the original work of Russell and Khalili (2006) and investigated the effect of hydraulic hysteresis and the influence of three drainage conditions (constant suction, constant moisture content, and χs condition, i.e., constant contribution of suction to the effective stress) on cavity pressure. The cavity creation problems were only considered in the analysis and the governing equations were solved using similarity technique proposed by Collins *et al.* (1992) and Collins and Stimpson (1994). They reported that hydraulic hysteresis has a negligible effect on the cavity expansion response and the simplified assumption of constant χs drainage condition is sufficient to yield a fairly accurate result irrespective of the actual drainage condition. Cheng *et al.* (2018) presented a new solution for cavity expansion problems in unsaturated

*Corresponding author, Assistant Professor
E-mail: sudheesh@iitpkd.ac.in
[a]Ph.D. Student
E-mail: alphalukose@gmail.com

ISSN: 2005-307X (Print), 2092-6219 (Online)

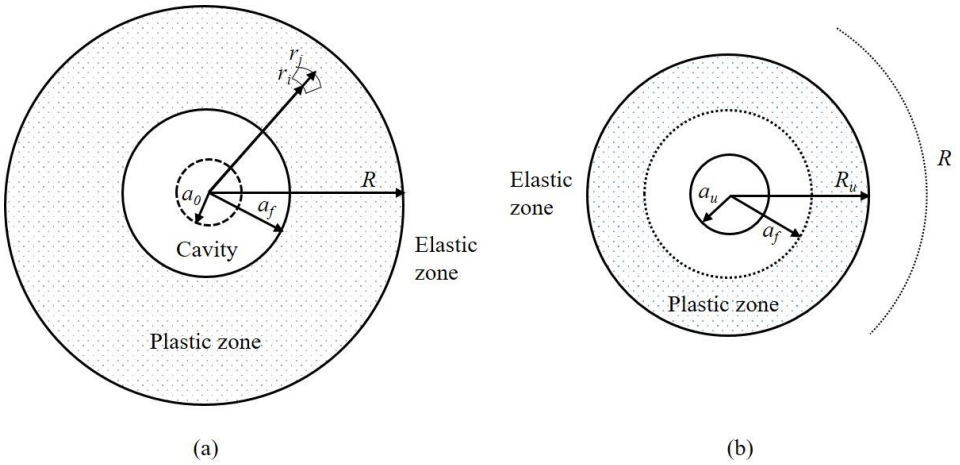

Fig. 1 Zones of: (a) an expanded cavity; and (b) contracted cavity

soils of finite radial extent, assuming a constant χs drainage condition and ignoring hydraulic hysteresis, specifically for the interpretation of calibration chamber studies. The stress - strain behaviour was modelled using elastic-plastic model and the plastic cavity expansion solution was formulated using the auxiliary independent variable proposed by Chen *et al.* (2013). Recently, Tang *et al.* (2021) developed a solution for spherical cavity expansion in unsaturated soils by considering constant suction condition. The cavity expansion problem was formulated as a system of first-order differential equations and this was solved as an initial value problem to obtain the unknown principal stress components and suction.

It is apparent that the published cavity expansion solutions in unsaturated soils either do not incorporate the soil-state-dependent variation of friction and dilation angles in the plastic zone or do not provide the distribution of soil state (stresses and soil properties) around a cavity corresponding to an expansion state other than the steady state condition (i.e., expansion under a constant limit pressure). Though the steady state condition is always reached in a cavity creation problem (e.g., cone penetration test, installation of driven piles, etc.), it may not be achievable during the finite expansion of a pre-existing cavity (e.g., pressuremeter tests, pressure-grouting of piles, tiebacks, and soil nails, etc.) (Salgado and Prezzi 2007, Thiyyakkandi *et al.* 2013, Zhao *et al.* 2018). Cavity contraction solution in unsaturated residual soil, integrating the effect of suction, though found to be highly instrumental in the interpretation of entire PMT data (Schnaid *et al.* 2000), has not been reported hitherto. These highlight the need for a new cavity expansion and contraction solutions for unsaturated residual soils, considering the effect of matric suction and variable friction and dilation angles as a function of soil-state, applicable for both cavity expansion as well as creation problems and unloading from any state of expansion (both steady-state and pre-steady state).

This paper presents a numerical solution procedure for cavity expansion and contraction problems in unsaturated residual soils, modelled as Mohr-Coulomb material, with the full incorporation of non-linear soil behaviour (i.e., hardening/softening). The proposed solution assimilates the influence of matric suction, large-strain effects, and variation of friction and dilation angles with soil-state within the plastic zone of expanding/contracting cavity. The numerical procedure adopted is similar to the one suggested by Salgado and Randolph (2001), wherein the plastic zone is discretized into cylindrical/spherical elements and the iterative approach proceed from the assumed elastic-plastic interface, element by element, toward the cavity wall. Such discretization approach for cavity contraction analysis was not found in any literature reviewed. The proposed approach considers constant contribution of suction to effective stress (constant χs drainage condition) and hydraulic hysteresis was ignored for simplicity based on the findings of Yang and Russell (2015a). To accentuate the in-field applicability of the proposed solution procedure, interpretation of pressuremeter test results (both loading and unloading) in residual soils (Schnaid *et al.* 2004) has been carried out. The solution approach was subsequently used to explore the general cavity expansion and contraction characteristics of unsaturated lateritic soil in Western Ghat region of India.

2. Cavity expansion and contraction formulation

2.1 Problem definition

Consider a cavity of initial radius a_0 in a homogeneous infinite soil mass initially under a hydrostatic stress state of p_0'. When an increasing internal pressure is applied, the cavity expands with the purely elastic deformation of the surrounding soil mass until the onset of plastic yielding of the cavity wall, which is governed by Mohr-Coulomb yield criterion. Beyond that, a plastic zone is formed around the cavity, which is enclosed by the elastic zones (non-linear and linear; Fig. 1(a)). The radius of cavity and radius of elastic - plastic boundary (R ; Fig. 1(a)) increases indefinitely as the internal pressure approaches to a limiting value known as the limit pressure (i.e., steady state condition). The steady state condition is not necessarily achieved during the finite cavity expansion of a pre-existing cavity. Hence, existing numerical formulations using self-

similarity technique (Collins *et al.* 1992, Salgado and Randolph 2001, Russell and Khalili 2006, Yang and Russell 2015a) could not be utilized for obtaining the variation of soil state within the surrounding soil mass. Such cavity expansion situations which do not involve steady state condition is termed here as *pre-steady-state* expansion. When the internal cavity pressure is released following the expansion to a pre-steady state or steady state condition, cavity contraction/unloading occurs from the expanded cavity radius a_f to a_u. Like the loading case, initial unloading response will be elastic in nature until the beginning of reverse plastic yielding. Thereafter, a reverse plastic zone (R_u) is formed around the cavity, diameter of which increases with further plastic unloading as depicted in Fig. 1(b).

2.2 Soil water characteristic curve and effective stress parameter

A well adopted method to incorporate unsaturated soil properties into cavity expansion analysis is to include matric suction in the formulation of solution; which can be done using soil-water characteristic curve, that represents the relationship between volumetric/gravimetric water content (θ or w) or degree of saturation (S), void ratio (e) and matric suction (s) of the soil (Fredlund and Xing 1994). The suction 's' is usually defined in terms of matric suction which is the difference of pore air pressure (u_a) and pore water pressure (u_w). Various models which relate variation in degree of saturation, void ratio and water content with suction are available in literature (Fredlund and Xing 1994, Russell and Buzzi 2012). The model adopted in this study is that proposed by Russell and Buzzi (2012), where hydraulic hysteresis is neglected

$$S = \begin{cases} 1 & \text{if} \quad s < s_e \\ (s/s_e)^{\alpha} & \text{if} \quad s > s_e \end{cases} \tag{1}$$

where s_e is the suction value at which soil changes from saturated to unsaturated state; $s_e = s_{ex}$ (air-expulsion value) when the hydraulic state is on the main wetting curve; $s_e = s_{ae}$ (air-entry value) when the hydraulic state is on the main drying curve; α is the slope of the curve, which is equal to (D_p - 3) for fractal soils, where D_p is the fractal dimension of soil pore size distribution (generally ranging from 2 to 3). The air-entry value, s_{ae}, varies with void ratio as (Russell 2014)

$$s_{ae} = C_1 \ e^{-\gamma}; \text{and} \quad s_{ex} = C_2 \ s_{ae} \tag{2}$$

where C_1 is a constant with units of stress; C_2 is a dimensionless constant; and γ is another dimensionless constant = D_s, the fractal dimension of the particle size distribution.

The effective stress (σ') in unsaturated soil is defined as

$$\sigma' = \sigma + \chi s \tag{3}$$

where σ is the total stress in excess of pore air pressure (u_a), also known as the net stress; χ is the effective stress parameter, which depend upon the degree of saturation (i.e., χ=1 for saturated soils and 0 for dry soils), is estimated here using the model (Eq. (4)) of Khalili *et al.* (2008).

$$\chi = \begin{cases} 1 & \text{if} \ \dfrac{s}{s_e} \leqslant 1 \\ (s/s_e)^{-\Omega} & \text{if} \ \dfrac{s}{s_e} \geqslant 1 \end{cases} \tag{4}$$

where Ω is material parameter with a best-fit value of 0.55.

2.3 Cavity expansion - Elastic zone

The equilibrium equation in terms of effective stress for spherical/cylindrical cavity in both elastic and plastic zones can be written as

$$\frac{d\sigma_r'}{dr} + \frac{k(\sigma_r' - \sigma_\theta')}{r} - \frac{d(\chi s)}{dr} = 0 \tag{5}$$

where σ_r' and σ_θ' are the effective radial and effective hoop stresses, respectively; the variable k denotes cylindrical (k = 1) or spherical (k = 2) case. Since constant χs condition is assumed throughout the expansion and contraction, Eq. (5) gets reduced to

$$\frac{d\sigma_r'}{dr} + \frac{k(\sigma_r' - \sigma_\theta')}{r} = 0 \tag{6}$$

The geomechanics sign convention of compressive stresses and strains as positive is followed in the paper.

Using the elastic stress-strain relationships, equilibrium equation (Eq. (6)) and boundary conditions (i.e., σ_r' (a) = p' and $\lim_{r\to\infty}\sigma_r' = p_0'$), the well-known solutions for stresses, strain and displacement in the elastic region can be obtained as

$$\sigma_r' = p_0' + (p' - p_0')\left(\frac{a}{r}\right)^{(k+1)} \tag{7}$$

$$\sigma_\theta' = p_0' - \frac{(p' - p_0')}{k}\left(\frac{a}{r}\right)^{(k+1)} \tag{8}$$

$$\varepsilon_r = \frac{(p' - p_0')}{2G}\left(\frac{a}{r}\right)^{(k+1)} \tag{9}$$

$$\varepsilon_\theta = -\frac{(p' - p_0')}{2Gk}\left(\frac{a}{r}\right)^{(k+1)} \tag{10}$$

$$u = -\varepsilon_\theta \quad r \tag{11}$$

where ε_r - radial strain; ε_θ - hoop strain; u - radial displacement; p_0' - effective in-situ hydrostatic stress ($p_0' = p_0 + \chi s$); a - cavity radius; p' - cavity pressure when cavity radius is a; r - radius of a material point and G - shear modulus.

The shear modulus of unsaturated residual soil has been reported to follow a power law decay as volumetric water content increases (Lu and Kaya 2014). Several empirical models for predicting the variation of shear modulus with volumetric water content or matric suction can be found in literature (Ng *et al.* 2009, Lu and Kaya 2014). Lu and Kaya (2014) proposed a simple power law model (Eq. (12)) with

a single curve fitting parameter (m)

$$G = G_d + (G_w - G_d)\theta_{eff}{}^m \tag{12}$$

where G_d and G_w are the shear modulus values at dry and wet state, respectively; θ_{eff} is the effective volumetric water content = $\left(\frac{\theta-\theta_d}{\theta_w-\theta_d}\right)$; θ, θ_d, θ_w are the volumetric water content values corresponding to the given condition, dry state and wet state, respectively.

The cavity pressure-expansion curve and the effective soil stresses, strains and radial displacement within the elastic zone till the onset of plastic yielding at the cavity wall can be obtained forthrightly using the elastic solutions (Eqs. (7)-(11)). The corresponding total stress values (σ_r, σ_θ) can be estimated subsequently by Eq. (3).

2.4 Cavity expansion - Plastic zone

During the internal loading, the cavity wall is assumed to yield when the stress state satisfies the Mohr-Coulomb criterion

$$\sigma_r' = \sigma_\theta' N_p + 2c'\sqrt{N_p} \tag{13}$$

where c' is the true effective cohesion intercept and N_p is the peak flow number, as given by

$$N_p = \frac{1+\sin\phi_p'}{1-sin\phi_p'} \tag{14}$$

where ϕ_p' is the peak effective friction angle, which is assumed to be independent of the degree of saturation of soil.

Once the cavity wall is yielded, further increase of the internal pressure causes the formation of distinct plastic and elastic zones around the cavity as discussed previously (Fig. 1(a)). For any thin shell element within the plastic zone bounded by inner radius, r_i, and outer radius r_j (Fig. 1(a)), an expression relating the effective inner radial stress (σ_{r_i}') and effective outer radial stress (σ_{r_j}') can be obtained by combining the equilibrium equation (Eq. (6)) and yield criterion (Eq. (13)) as follows

$$\sigma_{r_i}' = \sigma_{r_j}' \left(\frac{r_j}{r_i}\right)^{\frac{(N_{ij}-1)k}{N_{ij}}} + \frac{2c_{ij}'\sqrt{N_{ij}}}{1-N_{ij}}\left[1-\left(\frac{r_j}{r_i}\right)^{\frac{(N_{ij}-1)k}{N_{ij}}}\right] \tag{15}$$

The effective inner hoop stress (σ_{θ_i}') can then be determined using Eq. (16)

$$\sigma_{\theta_i}' = \frac{\sigma_{r_i}'}{N_{ij}} - \frac{2c_{ij}'}{\sqrt{N_{ij}}} \tag{16}$$

where N_{ij}= $\frac{1+sin\phi_{ij}'}{1-sin\phi_{ij}'}$, is the flow number and ϕ_{ij}' is the effective friction angle and c_{ij}' is the effective cohesion within the shell element ij.

The simplified Davis (1969) expression for mean effective stress in frictional soil given in Salgado and Randolph (2001) was extended for cohesive-frictional soils. This was used to estimate mean effective stress within each shell element, incorporating the third principal stress component as given below

$$p_m' = \frac{1}{3}\left\{\left[\bar{\sigma_r}'\left(1+\frac{k}{N_{ij}}\right)\left(1+\mu_{ij}(2-k)\right)\right] - \left[\frac{2c_{ij}'}{\sqrt{N_{ij}}}\left(1+\mu_{ij}(2-k)\right)k\right]\right\} \tag{17}$$

where $\bar{\sigma_r}'$ is the average radial stress of the element [(σ_{r_i}' + σ_{r_j}') / 2]; and $\mu_{ij} = 0.5(1 + sin\phi_{ij}' sin\psi_{ij})$ for k =1. The dilatancy rate, $\sin\psi_{ij}$, is assumed to hold the relation, Eq. (18) (Schanz and Vermeer 1996)

$$sin\,\psi_{ij} = \frac{sin\,\phi_{ij}' - sin\,\phi_c'}{1 - sin\,\phi_{ij}'\,sin\,\phi_c'} \tag{18}$$

The friction angle, which varies across the plastic zone of an expanding cavity, is assumed to vary according to the state parameter model, Eq. (19), (Been and Jefferies 1985) proposed for sand. It was evident from Been and Jefferies (1985) that the effect of variation of confining stress on shear strength can be modelled commendably using state parameters

$$\phi_{ij}' = \phi_c' + A\left[e^{-\xi_{ij}} - 1\right] \tag{19}$$

where A = constant which depends on characteristics of soil and type of loading; ξ_{ij} is the state parameter within the element ij and given by

$$\xi_{ij} = \upsilon_{ij} + \lambda\, ln\left(\frac{p_m'}{p_1}\right) - \Gamma \tag{20}$$

where υ_{ij}=1+e_{ij} is the specific volume, e_{ij} is the void ratio and p_m' is the mean effective stress (Eq. (17)) within the element ij; p_1 is the reference stress = 1 kPa (generally); and λ and Γ are the slope and intercept of critical state line in υ- $ln\ \ p$ plot.

From the stress – dilatancy relation for non-associated cohesive- frictional soil proposed by Zhang and Salgado (2010), it can be found that

$$N_{ij} = N_c D_{ij} \tag{21}$$

where N_c= $\frac{1+sin\phi_c'}{1-sin\phi_c'}$ is the flow number corresponding to the critical state friction angle (ϕ_c'); and D_{ij} is strain rate ratio within the shell element ij, which is given by

$$D_{ij} = 1 - \left(\frac{\dot{\varepsilon}_v}{\dot{\varepsilon}_1}\right) \tag{22}$$

where $\dot{\varepsilon}_v$ and $\dot{\varepsilon}_1$ are the volumetric strain rate and major principal strain rate, respectively; once ϕ_{ij}' is known from Eq. (19), D_{ij} for the element can be determined using Eq. (21). In case of cavity expansion, Eq. (22) can be expressed in incremental form as

$$D_{ij} = 1 - \frac{\varepsilon_v{}^{(i)} - \varepsilon_v{}^{(j)}}{\varepsilon_r{}^{(i)} - \varepsilon_r{}^{(j)}} \tag{23}$$

The strain components are defined as logarithmic strains

as given below (Eqs. (24)–(26)) so as to take into account large deformation in the plastic zone.

$$\varepsilon_r^{(i)} = -ln\left(\frac{r_j - r_i}{(r_j - u_j) - (r_i - u_i)}\right) \tag{24}$$

$$\varepsilon_\theta^{(i)} = \varepsilon_\varphi^{(i)} = -ln\left(\frac{r_i}{r_i - u_i}\right) \tag{25}$$

$$\varepsilon_v^{(i)} = -ln\left(\frac{{r_j}^{(k+1)} - {r_i}^{(k+1)}}{[r_j - u_j]^{(k+1)} - [r_i - u_i]^{(k+1)}}\right) \tag{26}$$

where u_i and u_j are radial displacements at r_i and r_j, respectively.

Plugging Eq. (24) and (26) in Eq. (23) with the assumption that the radial and volumetric strains of the previous element (${\varepsilon_r}^{(j)}$ and ${\varepsilon_v}^{(j)}$) are known and simplifying gives

$$\begin{aligned}&{\varepsilon_v}^{(j)} + (D_{ij} - 1){\varepsilon_r}^{(j)} \\ &= ln\left\{\left[\frac{(r_j - u_j)^{k+1} - (r_i - u_i)^{k+1}}{{r_j}^{k+1} - {r_i}^{k+1}}\right]\cdot\left[1 + \frac{u_i - u_j}{r_j - r_i}\right]^{D_{ij}-1}\right\}\end{aligned} \tag{27}$$

The radial displacement (u_i) at the inner boundary of the element ij can be determined by solving the above equation iteratively. Subsequently, ${\varepsilon_r}^{(i)}$, ${\varepsilon_\theta}^{(i)}$, and ${\varepsilon_v}^{(i)}$ can be obtained using Eqs. (24)-(26).

The expressions for effective radial and hoop stresses, radial and hoop strains and displacement at the elastic-plastic boundary (i.e., r = R) can be derived by making use of Eqs. (7)-(11) and (13), as summarized below.

$$\sigma_R' = \frac{[p_0'(N_p(k+1)] + [2c'\sqrt{N_p}]k}{(k + N_p)} \tag{28}$$

$$\sigma_\Theta' = \frac{\sigma_R'}{N_p} - \frac{2c'}{\sqrt{N_p}} \tag{29}$$

$$\epsilon_R = \frac{[2c'\sqrt{N_p} + p_0'(N_p - 1)]k}{2G(k + N_p)} \tag{30}$$

$$\epsilon_\Theta = -\frac{[2c'\sqrt{N_p} + p_0'(N_p - 1)]}{2G(k + N_p)} \tag{31}$$

$$u_R = \frac{[2c'\sqrt{N_p} + p_0'(N_p - 1)]r}{2G(k + N_p)} \tag{32}$$

2.5 Cavity contraction – Elastic unloading

As mentioned earlier, during cavity contraction subsequent to expansion, the initial response is elastic satisfying the equilibrium equation (Eq. (6)). The equations for effective stress, strain, and displacement components at any material point at a radial distance of r_u (which was at r before unloading) can be directly deduced by modifying Eq. (7) through (11) as given below

$$\sigma_{ru}' = \sigma_r' - (p_f' - p_u')\left(\frac{a_u}{r_u}\right)^{(k+1)} \tag{33}$$

$$\sigma_{\theta u}' = \sigma_\theta' + \frac{(p_f' - p_u')}{k}\left(\frac{a_u}{r_u}\right)^{(k+1)} \tag{34}$$

$$\varepsilon_{ru} = -\frac{(p_f' - p_u')}{2G}\left(\frac{a_u}{r_u}\right)^{(k+1)} \tag{35}$$

$$\varepsilon_{\theta u} = \frac{(p_f' - p_u')}{2Gk}\left(\frac{a_u}{r_u}\right)^{(k+1)} \tag{36}$$

$$u_u = -\varepsilon_{\theta u} \quad r_u \tag{37}$$

where p_f' is the cavity pressure at the end of loading; p_u' is the current cavity pressure; a_u is the current radius of cavity.

The cavity wall subjects to reverse yielding when σ_{ru}' and $\sigma_{\theta u}'$ at the cavity wall follow the reverse Mohr-Coulomb yield criterion

$$\sigma_{\theta u}' = \sigma_{ru}' N + 2c'\sqrt{N} \tag{38}$$

where N is the flow number and c' is the effective cohesion at the cavity wall at the end of expansion.

This will happen when the effective cavity pressure is equal to

$$p_r' = \frac{p_f'\ (N + k) - 2c'\sqrt{N}(N + 1)k}{N(Nk + 1)} \tag{39}$$

2.6 Cavity contraction – Plastic unloading

Following the reverse yielding of cavity wall, a reverse plastic zone is formed around the cavity, radius (R_u) of which increases with further unloading (Fig. 1(b)). Similar to Eq. (15), a relationship between the effective inner radial stress (σ_{ru_i}') and effective outer radial stress (σ_{ru_j}') can be derived for any thin element (ij) within the reverse plastic zone with the aid of equilibrium equation (Eq. (6)) and reverse yield criterion (Eq. (38))

$$\begin{aligned}\sigma_{ru_i}' = \sigma_{ru_j}'\left(\frac{r_{u_j}}{r_{u_i}}\right)^{(1-N_{ij})k} \\ - \frac{2c_{ij}'\sqrt{N_{ij}}}{N_{ij} - 1}\left[1 - \left(\frac{r_{u_j}}{r_{u_i}}\right)^{(1-N_{ij})k}\right]\end{aligned} \tag{40}$$

Then the effective inner hoop stress ($\sigma_{\theta u_i}'$) can be obtained as

$$\sigma_{\theta u_i}' = \sigma_{ru_i}' N_{ij} + 2c_{ij}'\sqrt{N_{ij}} \tag{41}$$

Like Eq. (17), an expression for the mean stress within an element during cavity contraction can be devised as given below

$$\begin{aligned}p_m' = \frac{1}{3}\{&[\bar{\sigma}_{ru}'(1 + kN_{ij})(1 + \mu_{ij}(2 - k))] \\ &+ [2c_{ij}'\sqrt{N_{ij}}(1 + \mu_{ij}(2 - k))k]\}\end{aligned} \tag{42}$$

The definition of strain rate ratio within the shell element, ij, as given by Eq. (22) can be utilized to derive

the expression for the displacement at the inner boundary (u_{u_i}) as follows

$$D_{u_{ij}} = 1 - \frac{{\varepsilon_{vu}}^{(i)} - {\varepsilon_{vu}}^{(j)}}{{\varepsilon_{\theta u}}^{(i)} - {\varepsilon_{\theta u}}^{(j)}} \tag{43}$$

Assuming that the hoop and volumetric strains of the previous element (${\varepsilon_{\theta u}}^{(j)}$ and ${\varepsilon_{vu}}^{(j)}$) are already known and substituting strains in terms of radii and displacement (similar to Eqs. (24)-(26)) in Eq. (43), yields

$$\begin{aligned} &{\varepsilon_{vu}}^{(j)} + (D_{u_{ij}} - 1){\varepsilon_{\theta u}}^{(j)} \\ &= ln\left\{\left[\frac{(r_{u_j} - u_{u_j})^{k+1} - (r_{u_i} - u_{u_i})^{k+1}}{{r_{u_j}}^{k+1} - {r_{u_i}}^{k+1}}\right].\left[\frac{r_{u_i} - u_{u_i}}{r_{u_i}}\right]^{D_{u_{ij}}-1}\right\} \end{aligned} \tag{44}$$

Solving the above equation gives, inner radial displacement (u_{u_i}), which can then be used to determine the strain components (${\varepsilon_{ru}}^{(i)}$, ${\varepsilon_{\theta u}}^{(i)}$ and ${\varepsilon_{vu}}^{(i)}$).

The effective radial stress (σ'_{Ru}), hoop stress ($\sigma'_{\Theta u}$), the strain components (ε_{Ru} and $\varepsilon_{\Theta u}$) and displacement (u_{Ru}) at the elastic-plastic boundary (radius = R_u) of a contracting cavity can be derived by following the similar approach adopted for the loading case:

$$\sigma'_{Ru} = \frac{\sigma'_l(N_{Ru} + k) - 2c'_{Ru}\sqrt{N_{Ru}}(N_{Ru} + 1)k}{N_{Ru}(N_{Ru}k + 1)} \tag{45}$$

$$\sigma'_{\Theta u} = \frac{\sigma'_l(N_{Ru} + k) - 2c'_{Ru}\sqrt{N_{Ru}}(k - 1)}{(N_{Ru}k + 1)} \tag{46}$$

$$\varepsilon_{Ru} = -\frac{(\sigma'_l - \sigma'_{Ru})}{2G} \tag{47}$$

$$\epsilon_{\Theta u} = \frac{\sigma'_l - \sigma'_{Ru}}{2Gk} \tag{48}$$

$$u_{Ru} = -\varepsilon_{\theta u}.R_u \tag{49}$$

where σ'_l is the effective radial stress at R_u at the end of loading; and c'_{Ru} and N_{Ru} are the effective cohesion and flow number at R_u, respectively.

3. Numerical implementation

A numerical procedure, utilizing all the necessary equations discussed in the previous section, was adopted to construct the entire pressure - expansion and contraction curve. The stress and displacement fields around a cylindrical/spherical cavity at any stage of loading or unloading can be obtained subsequently. The whole procedure has been subdivided into four distinct sections based on loading or unloading and elastic or elastic-plastic response as, (i) elastic loading; (ii) plastic loading; (iii) elastic unloading; and (iv) plastic unloading. One explicit assumption made is that the soil's SWCC, critical state parameters, and initial soil state are available. The entire algorithm is summarized below:

a) Choose input parameters:
   (i) Physical properties: initial void ratio (e_0), moisture content (w) or initial degree of saturation (S_0), and specific gravity (G_s)
   (ii) SWCC parameters
   (iii) Strength and stiffness parameters: c', ϕ'_c, G (Eq. (12)), and υ
   (iv) Input for state parameter model: A, λ, and Γ
   (v) In-situ stress (p_0)
   (vi) k = 1 or 2 (for cylindrical or spherical, respectively)
   (vii) Initial cavity radius (a_0)
   (viii) Final cavity radius at the end of loading (a_f) or final loading cavity pressure (p'_f); whichever controls the termination of the expansion process

Elastic loading: For any internal pressure (p') less than the pressure to initiate yielding, p'_y (= σ'_R), the response of surrounding soil is elastic in nature.

b) Calculate the peak friction angle (ϕ'_p) at the elastic-plastic boundary through an iterative procedure as follows: Initially assume a suitable value of ϕ'_p and determine N_p using Eq. (14). Subsequently, calculate σ'_R at elastic-plastic boundary from Eq. (28) and then, the mean stress using Eq. (17). Using this mean stress, calculate the new value of ϕ'_p by Eq. (19). Repeat the entire process with the new ϕ'_p until sufficient convergence is obtained.
c) Calculate the effective stress (σ'_R, σ'_Θ), strain (ε_R, ε_Θ), and displacement (u_R) components at the elastic- plastic boundary using Eqs. (28) through (32).
d) Calculate hoop strain and radial displacement (u) at the cavity wall using Eqs. (10) and (11), respectively and then determine the corresponding radius of cavity as, $a = a_0 + u$ for $p' \le p'_y$. At yielding (i.e., $p' = p'_y$), cavity radius, $a_y = a_0 + u_y$.
e) Use elastic solutions (Eqs. (7) through (11)) to determine the effective stress, strain, and displacement fields around the cavity, if required.

Plastic loading: For $p' > p'_y$, a plastic zone is formed around the cavity, which expands with further loading. Since friction and dilation angles vary across the plastic zone, a recursive approach similar to that proposed by Salgado and Randolph (2001) is adopted here to incorporate non-linear soil response. In this approach, the plastic zone is discretised into thin shell elements and the analysis is advanced inward from the elastic-plastic boundary, where the stress, strain and displacement values are already known (Step c), element by element to the cavity wall. The detailed procedure and flowchart (Fig. 2) are given below:

f) Choose a plastic radius, R_1, greater than a and subdivide the plastic zone into very thin elements (thickness = dr).
g) Start with the first element (ij) with outer boundary (j) at R_1, where all the parameters are known (σ'_{r_j}, σ'_{θ_j}, ${\varepsilon_r}^{(j)}$, ${\varepsilon_\theta}^{(j)}$, ${\varepsilon_v}^{(j)}$, and u_j). The outer and inner radii of

the element are r_j and r_i, respectively; i.e., $r_i = r_j - dr$. Initially assume that friction angle, ϕ'_{ij} and cohesion, c'_{ij} of the first element are the same as the values at R_1.

(i) Calculate the effective inner radial stress (σ'_{r_i}) using Eq. (15), effective inner hoop stress (σ'_{θ_i}) from Eq. (16) and mean stress (p'_m) for the element through Eq. (17).
(ii) Estimate the strain rate, D_{ij} from Eq. (21).
(iii) Solve Eq. (27) for inner radial displacement (u_i) as all other parameters in the equation are known. Newton-Raphson iteration method is used here for solving the equation.
(iv) Find ${\varepsilon_r}^{(i)}$, ${\varepsilon_\theta}^{(i)}$, and ${\varepsilon_v}^{(i)}$ from Eqs. (24) – (26).
(v) Determine new D_{ij} using Eq. (23).
(vi) Calculate void ratio (e_{ij}) of the element: $e_{ij} = \frac{1+e_0}{\exp({\varepsilon_v}^{(i)})} - 1$.
(vii) Calculate new ϕ'_{ij} from Eq. (19).
(viii) Repeat the iteration (i to vii) for the first element until the required convergence for ϕ'_{ij} is achieved. Then all the parameter at the inner boundary (i) will be known.

h) Repeat Step (g) for next element and proceed element by element inward. Note that the parameters at the outer boundary of an element will correspond to that at the inner boundary of the previous element. After achieving convergence for each element, $r_i - u_i$ is compared with the initial cavity radius (a_0). If $r_i - u_i > a_0$, carry forward with the next element; whereas, if $r_i - u_i \approx a_0$, cavity wall is reached and then, new cavity radius, $a_1 = r_i$ and new effective internal pressure, $p'_1 = \sigma'_{r_i}$. The (u_1, p'_1) set represents the first data point on the pressure-expansion curve following the plastic yielding point (u_y, p'_y).
i) Repeat Steps (f) through (h) by gradually increasing the plastic radius as R_2, R_3, ..., R_n. Calculations with each plastic radius will yield each set of data point for the pressure-expansion curve. This process is continued until the required final condition has been reached; i.e., steady state condition or the required expansion radius (a_f) or effective cavity pressure (p'_f), depending on whichever is the termination criterion.
j) This iterative process will yield the stress, strain, and displacement fields as well as the variation of soil properties (friction and dilation angles, void ratio, etc.) within the plastic zone at any stage of expansion (i.e., corresponding to R_1, R_2,..., R_n). The distribution of stress, strain and displacement outside the plastic zone can be obtained using the elastic solutions (Eqs. (7) through (11)) by substituting $a = R$ and $p' = \sigma'_R$.

Elastic unloading: Unloading from any state of cavity loading or expansion is considered here and the soil state at the end of loading phase is taken as the reference condition. For any decrease of internal pressure from p'_f (at end of loading) to p'_u until the onset of reverse yielding (p'_r), the response is purely elastic.
k) Calculate the effective cavity pressure at the onset of reverse yielding (p'_r) from Eq. (39).
l) Determine hoop strain and radial displacement (u_u) at the cavity wall using Eqs. (36) and (37), respectively for any $p'_u \le p'_r$. The corresponding radius of cavity can be then estimated as, $a_u = a_f + u_u$; at reverse yielding, $a_{ur} = a_f + u_{ur}$.
m) The distribution of stresses, strains and displacement in the soil surrounding the cavity can be obtained using the elastic solutions, Eqs. (33)-(37).

Plastic unloading: Further unloading (i.e., $p'_u < p'_r$), causes development of a reverse plastic zone near the cavity, radius of which increases with the unloading. A numerical procedure similar to that followed for plastic loading was used to account for the evolution of soil state as summarized below along with a flowchart representation (Fig. 3):

n) Choose a reverse plastic radius, R_{u1}, greater than a_{ur} and discretize the reverse plastic zone into thin shell elements (thickness = dr).
o) Calculate all the parametric values (σ'_{Ru}, $\sigma'_{\Theta u}$, ε_{Ru}, $\varepsilon_{\Theta u}$, and u_{Ru}) at the elastic-plastic boundary, R_{u1}, using Eqs. (45) through (49).
p) Consider the first element (ij) inside R_{u1}, for which the friction angle, ϕ'_{ij} and cohesion, c'_{ij} are initially assumed to be the same as at the end of loading phase.

(i) Calculate effective inner radial stress (σ'_{ru_i}), effective inner hoop stress ($\sigma'_{\theta u_i}$) and mean stress (p'_m) successively using Eqs. (40) through (42).
(ii) Determine the inner radial displacement (u_{ui}) by solving Eq. (44).
(iii) Calculate ${\varepsilon_{ru}}^{(i)}$, ${\varepsilon_{\theta u}}^{(i)}$, and ${\varepsilon_{vu}}^{(i)}$ from Eqs. (24) – (26).
(iv) Determine new $D_{u_{ij}}$ using Eq. (43).
(v) Calculate void ratio (e_{ij}) and new ϕ'_{ij} using Eq. (19).
(vi) Reiterate (i) to (v) until the ϕ'_{ij} from the two consecutive iterations are very close. Then all the parameter at the inner boundary (i) will be known.

q) Go to the next element and follow Step (p). Once the convergence is achieved for each element, $r_{ui} - u_{ui}$ is compared with the cavity radius at the end of loading phase (a_f). If $r_{ui} - u_{ui} > a_f$, proceed to the next element. If $r_{ui} - u_{ui} \approx a_f$, cavity wall has been reached and the corresponding new cavity radius, $a_{u1} = r_{ui}$, displacement, $u_{u1} = u_{ui}$, and effective cavity pressure, $p'_{u1} = \sigma'_{ru_i}$.
r) Repeat Steps (n) to (q) with the increase of reverse plastic radius in small increments (R_{u2}, R_{u3}, ..., R_{un}) to obtain the data sets for the entire pressure-contraction curve.

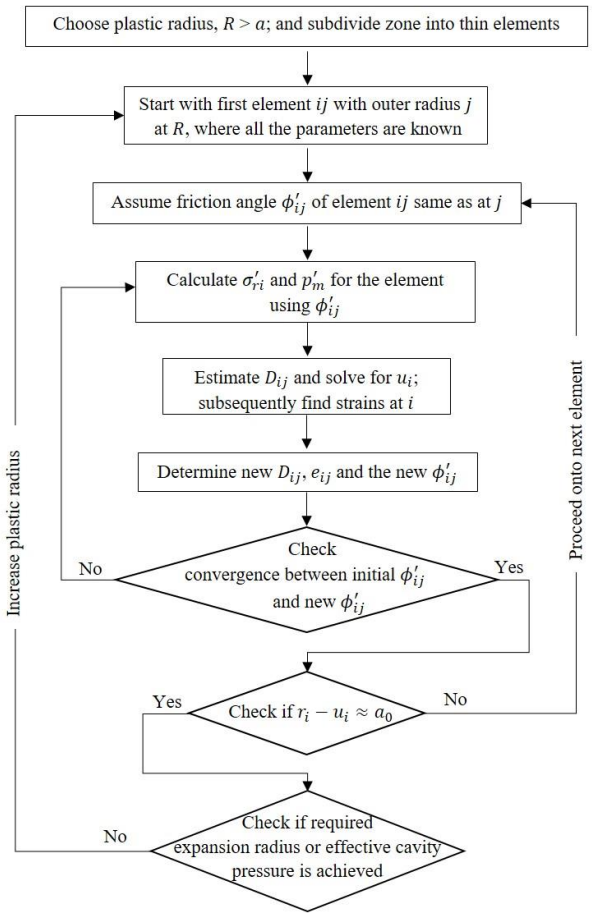

Fig. 2 Flowchart for numerical implementation of plastic loading

s) The variation of soil state (soil properties and stress state) within the reverse plastic zone at any stage of contraction (i.e., with reverse plastic radius: R_{u2}, R_{u3}, ..., R_{un}) will be known from the recursive procedure adopted here. The elastic solutions (Eqs. (33) -(37)) can be used to capture the stress and strain distribution beyond the reverse plastic region by replacing a_u, p'_f, and p'_u by R_u, σ'_l, and σ'_{Ru} respectively.

Note that all the stress outputs from the algorithm are the effective stresses; corresponding total stress components can subsequently be estimated following Eq. (3).

4. Validation

To validate the proposed solution, interpretation of pressuremeter test data in residual soil has been carried out. The results of suction monitored pressuremeter tests (SMPMT) in weak erodible yellow granite residual soil in Porto Alegre, southern Brazil, reported by Schnaid *et al.* (2004) were used for the same. Schnaid *et al.* (2004) have presented a detailed field and laboratory test program in unsaturated granite residual soils, including a series of pressuremeter tests (PMT) in pre-bored holes with suction monitoring using tensiometers at radial distances of 5D and 10D from the axis of borehole. This residual soil falls in the range of clayey sand to silty sand as per the Unified Soil Classification System (Schnaid *et al.* 2004).

Two SMPMT results in yellow granite residual soil at 2 m depth corresponding to, (a) initial suction, s_0 = 0 (saturated case); and (b) s_0 = 43 kPa (unsaturated case) were considered in the present study. Theoretical pressure – expansion/contraction curves for these two cases were produced by the proposed approach using the following input parameters obtained from the laboratory experiments (Schnaid *et al.* 2004): ϕ'_c = 36^0; ϕ'_p = 43^0; c' = 1 kPa; υ = 0.24 and 0.3 for unsaturated and saturated cases, respectively; G_s = 2.63; e_0 = 0.9; χ = 0.5; $S_{0\ (s_0\ =\ 0)}$=88%, $S_{0\ (s_0\ =\ 43\ \mathrm{kPa})}$ = 58% (from SWCC). The critical state parameters (λ = 0.14; Γ = 2.6) adopted were the average values reported for Brazilian residual soils (Futai *et al.* 2004, Latib *et al.* 2018). The constant A (= 0.94) was back calculated using Eq. (19) with the known values of ϕ'_c and ϕ'_p. The ψ_p was estimated as 9^0 by Eq. (18). The shear modulus estimated from the elastic unloading portion of the PMT data was used as the original input for both loading and unloading analyses (G_l and G_u). The values were subsequently adjusted in the curve-fitting process until an adequate match between the predicted and measured responses was achieved. Fig. 4 displays the predicted pressure – expansion/contraction curves and the experimental PMT curves (Schnaid *et al.* 2004).

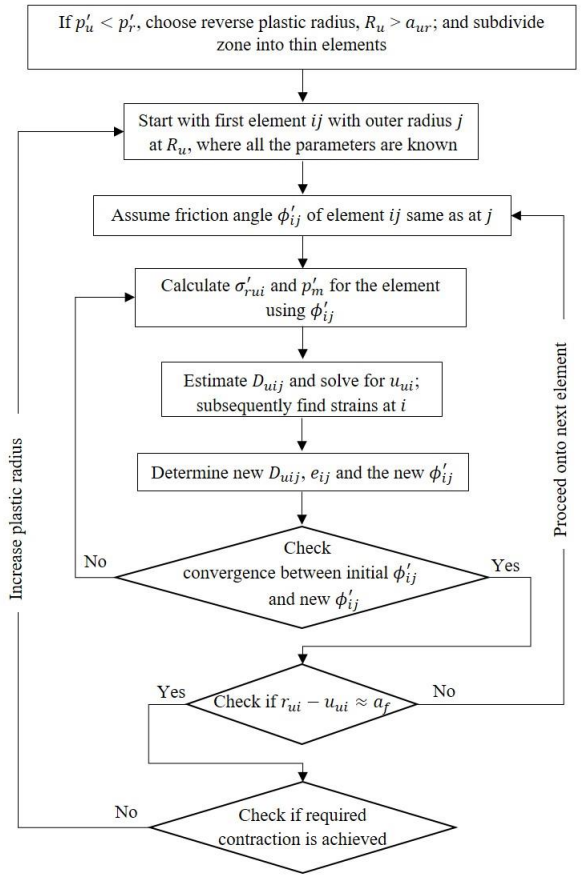

Fig. 3 Flowchart for numerical implementation of plastic unloading

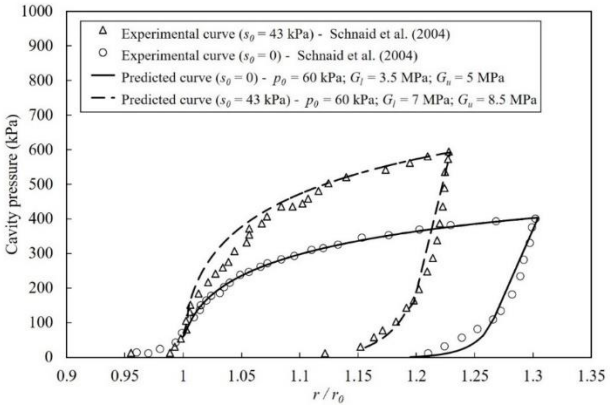

Fig. 4 Comparison of predicted and measured PMT responses in yellow granite residual soil

As evident from the figure, the predicted responses were in good agreement with the measured data (correlation coefficient, R^2 = 0.99 and 0.97 for s_0 = 0 and s_0 = 43 kPa, respectively), which confirms the validity of the proposed approach. The G_l values were found to be lower than the G_u values (17 - 30% less; Fig. 4), which may be attributed to the soil disturbance associated with the pre-boring of the test hole. The present comparison also verifies that the proposed expansion and contraction solutions can be used for the back-computation of soil's shear strength and stiffness parameters by adequately curve-fitting the entire PMT data.

5. Cavity expansion and contraction features of Western Ghat lateritic soil

5.1 Input parameters

The proposed solution approach was subsequently used to obtain the typical features of cavity expansion and contraction in unsaturated lateritic soil found in the Western Ghat region of Kerala State, India. A detailed laboratory testing of this soil was performed as per ASTM test procedures to determine its geotechnical characteristics.

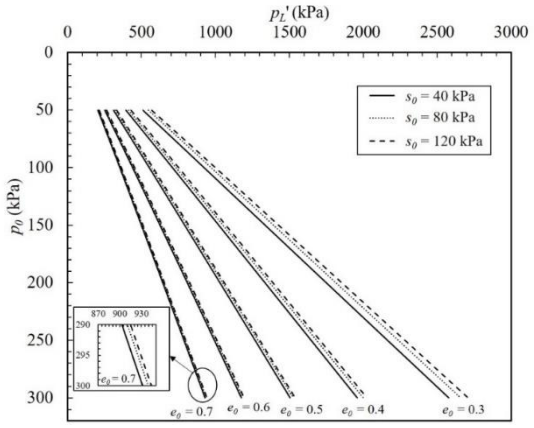

Fig. 5 Limit pressure versus p_0 for different e_0 and s_0 values in case of cylindrical cavity

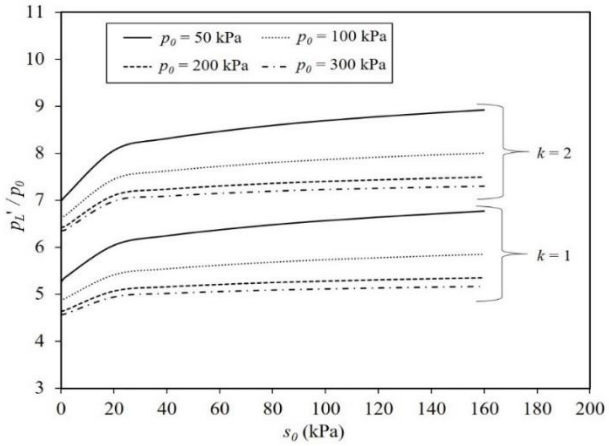

Fig. 6 Normalized limit pressure versus s_0 (e_0 = 0.5)

According to Unified Soil Classification System (USCS), the soil was classified as clayey sand (SC). The shear strength (ϕ_c', ϕ', c') and critical state parameters (λ, Γ and A) were obtained through a series of drained direct shear tests with different degree of saturations (0 - 99%) or volumetric water contents (0 - 33%) and normal stresses (25 - 200 kPa). However, the change in degree of saturation was found to have negligible influence on ϕ', $\phi_c{}'$, λ, Γ and A. The shear modulus (G) of soil obtained from the drained direct shear tests carried out with different initial degree of saturation was found to vary with the volumetric water content approximately as per the following expression (Eq. (50))

$$\frac{G}{{\sigma_m'}^{1.2}} = 30.6 - 14.6 \quad \theta_{eff} \tag{50}$$

where σ_m' is the mean effective stress and θ_{eff} is the effective volumetric water content which was obtained as $\left(\frac{\theta-\theta_d}{\theta_w-\theta_d}\right)$. It can be seen that Eq. (50) is identical to Eq. (12) with G_d = 30.6 ${\sigma_m'}^{1.2}$, G_w = 16 ${\sigma_m'}^{1.2}$ and the fitting parameter, m = 1 (i.e., linear variation). Eq. (50) can be used to calculate the input shear modulus of this soil corresponding to the given volumetric water content or degree of saturation.

Table 1 Parameters of lateritic soil

Parameter	Value
% of gravel	0
% of sand	69
% of fines	31
Liquid limit (%)	28.5
Plastic limit (%)	20
Plasticity index (%)	8.5
Specific gravity (G_s)	2.65
$\phi_c'(\ ^o)$	32
c' (kPa)	8
A	1.05
Γ	1.352
λ	0.015
Ω	0.55
α	-0.255
C_1	0.28
γ	2.6

Table 1 summarizes the relevant parameters obtained from the experimental investigation. Drying Soil Water Characteristic Curve (SWCC) for the soil was determined using the filter paper technique as per ASTM D5298 – 16 and the experimental data was fitted using Russell and

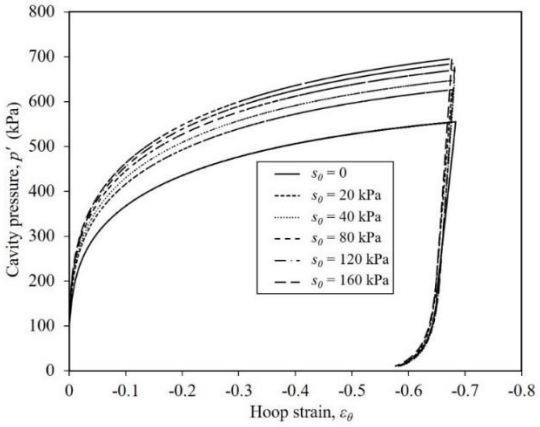

Fig. 7 Cylindrical cavity expansion and contraction curves for different s_0 (p_0 = 100 kPa, e_0 = 0.4, a_f/a_0 = 2)

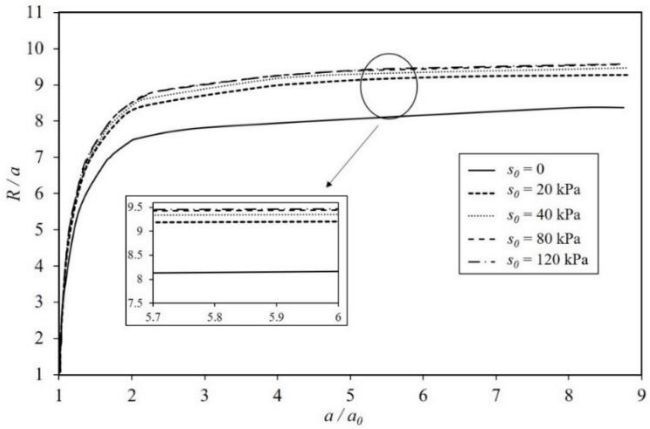

Fig. 8 R/a as a function of a/a_0 for cylindrical cavity (p_0 = 100 kPa, e_0 = 0.4)

Buzzi (2012) model; the obtained SWCC parameters are given in Table 1. The grain size distribution of the soil is fractal with a fractal dimension, D_s = 2.6 and s_{ae} as a function of the void ratio by $s_{ae} = 0.28e^{-2.6}$ kPa.

Cavity expansion and contraction simulations were then performed using the estimated parameters (Table 1) for a range of initial soil states: p_0 = 50 kPa to 300 kPa, e_0 = 0.2 to 0.7 and s_0 = 0 to 160 kPa. Subsequently, various plots were generated using the results to examine the influence of initial soil states (more importantly s_0) on the cavity expansion and contraction characteristics of this soil as presented below.

5.2 Cavity limit pressure

The cylindrical cavity limit pressure values (p_L') are plotted as a function of p_0 for a range of e_0 and s_0 in Fig. 5. The initial suction adopted are: s_0 = 40 kPa, 80 kPa, and 120 kPa and e_0 = 0.3, 0.4, 0.5, 0.6, and 0.7. As can be seen in Fig. 5, for any given initial soil state (i.e., p_0 and e_0), the limit pressure increases with increase in initial suction because of the increased initial mean effective stress. However, the effect of suction is found to be more pronounced in case of lower initial void ratios. Similar result was observed in case of spherical cavity limit pressure as well. For example, an increase of suction from 40 kPa to 120 kPa causes an increase in the cylindrical cavity limit pressure by 8.2% for the case of e_0 = 0.3; while the increase is only 2.5% for e_0 = 0.7 under the same initial stress state, p_0 = 100 kPa. This is due to the higher angle of internal friction at the elastic-plastic boundary at lower void ratio, which increases the apparent cohesion effect. The variation of normalized limit pressure (p_L'/p_0) against s_0 for cylindrical and spherical expansion cases for different p_0 conditions is shown in Fig. 6. It can be noticed from the figure that with the increase in p_0, the effect of suction on limit pressure becomes less significant due to the reduced relative contribution of suction to the effective stress as reported by Russell and Khalili (2006).

5.3 Cavity pressure - expansion / contraction curve

The theoretical pressure-expansion-contraction curves corresponding to a given expansion ratio (a_f/a_0) can effectively be utilized for the interpretation of the entire pressuremeter test results to back-compute the in-situ soil state as discussed previously. Unlike the existing methods for unsaturated soils, the proposed solution procedure allows modelling of unloading after any stage of expansion while incorporating the evolution of soil state during both expansion and contraction. Fig. 7 shows typical cylindrical cavity expansion and contraction curves for different s_0 values corresponding to an expansion ratio (a_f/a_0) of 2 (p_0 = 100 kPa and e_0 = 0.4). As evident from Fig. 7, suction

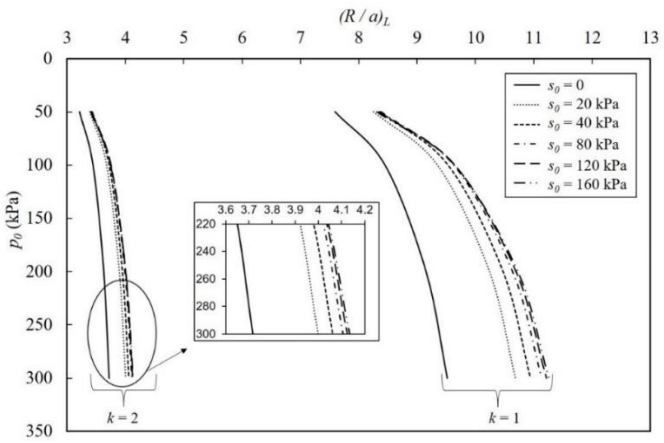

Fig. 9 Limiting normalized plastic radius, $(R/a)_L$ versus p_0 for cylindrical and spherical cavity expansions

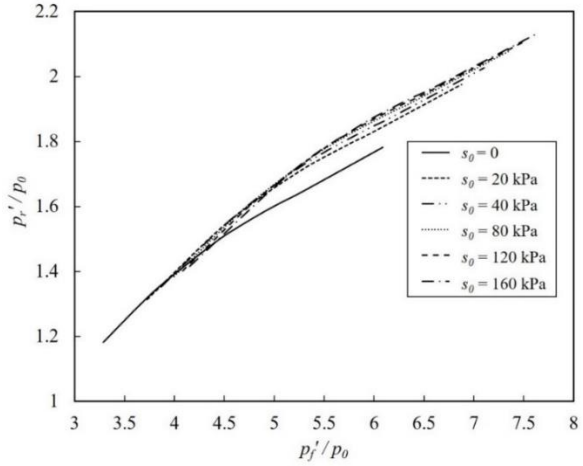

Fig. 10 (p_r'/p_0) versus (p_f'/p_0) at p_0 = 100 kPa and e_0 = 0.4

results in a stiffer response due to the increased effective stress and apparent cohesion. However, the rate of increase in cavity pressure decreases with increase in s_0, as effective stress parameter (χ) is inversely proportional to suction (Eq. (4)). Similar results were observed in case of spherical cavity expansion and contraction as well.

5.4 Plastic radius

The variation of normalized plastic radius (i.e., ratio of plastic radius to cavity radius; R/a) with the expansion ratio (a/a_0) for a cylindrical cavity at p_0 = 100 kPa and e_0 = 0.4 is shown in Fig. 8. It is evident from the figure that the rate of increase of R/a ratio is more pronounced up to an expansion ratio (a/a_0) of 2 and beyond that the rate of increase is marginal. It can also be found from Fig. 8 that R/a increases with the increase in s_0; however, the rate of change of R/a decreases with the increase in s_0. For example, an increase of s_0 from 0 to 20 kPa caused to increase R/a by 8% for spherical cavity and 12% for cylindrical cavity; the increase in R/a due to the further increase in s_0 was not significant. Fig. 9 shows the normalized plastic radius corresponding to the steady-state condition $[(R/a)_L]$ as a function of p_0 for different s_0 values. The initial void ratio, e_0 was taken as 0.4 for all the curves. It can be observed from the figure that $(R/a)_L$ ratio for a spherical cavity is relatively small when compared with that for a cylindrical cavity. Similarly, the rate of increase of $(R/a)_L$ with p_0 is not significant for the spherical cavity case in comparison with the cylindrical cavity case. For a given s_0 value, the effect of suction on $(R/a)_L$ was found to increase with the increase in p_0. The variation of plastic radius for different initial suction (Figs. 8 and 9) can be helpful while designing test chambers for model studies (e.g., pile installation and loading, grouting, calibration studies, etc.) in this or similar lateritic soils. Since the plastic zone radius for saturated and unsaturation conditions are different, boundary effect can also be different if sufficient boundary distances are not provided.

5.5 Reverse yield pressure

Fig. 10 presents the variation of normalized cylindrical cavity pressure at the onset of reverse yielding (p_r'/p_0) versus the normalized cavity pressure at the end of expansion (p_f'/p_0) for different s_0 values (p_0 = 100 kPa, e_0 = 0.4). The suction was found to increase the reverse yield pressure, p_r' (Fig. 10), though the rate diminishes

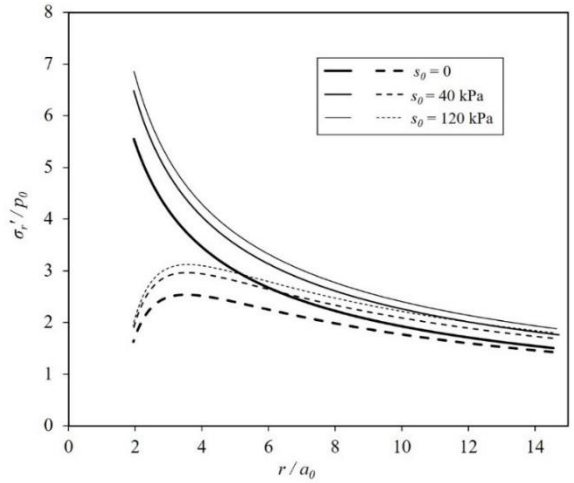

Fig. 11 Radial stress distribution around a cylindrical cavity (p_0 = 100 kPa, and e_0 = 0.4): (a) after expansion (a_f/a_0=2) [—]; and (b) at the end of elastic unloading [- - -]

with its increase as in the case of p_L'. For a given s_0 value, the influence of suction on p_r' is proportional to p_f'. The theoretical variation of p_r' with p_f' (Fig. 10) for the given in-situ soil state (p_0, e_0, and s_0) will help in deciding the safe unloading pressure to obtain unload-reload loops from pressuremeter tests.

5.6 Radial stress distribution

The prediction of stress state around a cavity at any stage of expansion or contraction is possible with the presented solution approach. Fig. 11 shows radial stress distribution around a cylindrical cavity at the end of expansion (a_f/a_0 = 2) and at the onset of reverse yielding for different s_0 values (p_0 = 100 kPa and e_0 = 0.4). The stress state prediction around an expanding or contracting cavity has numerous applications; for example, this would enable estimating the stress field around a tunnel, residual stress state and thus skin resistance of piles, tie backs, and soil nails subsequent to the installation and grouting, soil improvement due to compaction grouting, etc. (Lee *et al.* 2012, Thiyyakkandi *et al.* 2013, Li *et al.* 2019c).

6. Conclusions

This paper presents cylindrical/spherical cavity expansion and contraction solution - procedure for unsaturated residual soils, incorporating the non-linear soil response associated with the evolution of soil state. In the proposed recursive approach, plastic radius is increased incrementally; for each plastic radius, the plastic region is discretised into thin elements and the calculation is progressed from the elastic-plastic boundary towards the center of cavity. Unlike the existing methods based on self-similarity technique, which only enable the prediction of soil state (stress, displacement, soil properties, etc.) at the limit condition, the presented solution procedure allows the prediction of all the parameters of interest around a cavity at any stage of expansion and subsequent contraction. Notably, the proposed solution procedure integrates the effect of suction and the variation of soil state on the cavity contraction as well as expansion responses. The efficacy of this solution approach for back-computing strength and stiffness parameters of unsaturated residual soil using the entire expansion-contraction curve was validated by the interpretation of pressuremeter test data. The predicted pressure expansion and contraction responses were in good agreement with the measured data.

Further, the influence of initial soil state on cavity expansion and contraction characteristics of lateritic residual soil along the Western Ghats, India was examined using the proposed procedure. Charts are provided as a reference for quick estimation of limit pressure corresponding to different initial soil states (p_0, e_0, and s_0) in this soil. It was observed that suction resulted in a stiffer response due to the increased mean effective stress. Though suction increases the cavity pressure required for a specified expansion, its effect was found to be more pronounced at lower p_0 and e_0 values. The rate of increase in cavity pressure was seen to decrease with the increase of suction. The loading plastic radii was also found to increase, but at a decreasing rate, with the increase in suction. For a given s_0, effect of suction on the plastic radius was observed to increase with the increase in p_0, which is more striking in the case of a cylindrical cavity than a spherical cavity. This suggests that suction can increase the boundary effect in test chamber studies. The reverse yield pressure was also found to exhibit a similar trend with the increase in suction, the prediction of which is vital to ensure that unloading-reloading loop is purely-elastic while performing a PMT.

Acknowledgments

The solution approach and findings presented in this paper was a part of research funded by Science and Engineering Research Board (SERB) Research Grant (No. CRG/2019/004335) from the Department of Science and Technology (DST), Government of India, which is gratefully acknowledged. The financial support provided to the first author by the Ministry of Human Resource

Development (MHRD), India, for completion of this work is also thankfully acknowledged.

References

Been, K. and Jefferies, M.G. (1985), "A state parameter for sands", *Géotechnique*, **35**(2), 99-112. https://doi.org/10.1680/geot.1985.35.2.99.

Cao, L.F., Teh, C.I. and Chang, M.F. (2002), "Analysis of undrained cavity expansion in elasto-plastic soils with non-linear elasticity", *Int. J. Numer. Anal. Meth. Geomech.*, **26**(1), 25-52. https://doi.org/10.1002/nag.189.

Carter, J.P., Booker, J.R. and Yeung, S.K. (1986), "Cavity expansion in cohesive frictional soils", *Geotechnique*, **36**(3), 349–358. https://doi.org/10.1680/geot.1986.36.3.349.

Chen, S.L. and Abousleiman, Y.N. (2013), "Exact drained solution for cylindrical cavity expansion in modified Cam Clay soil", *Geotechnique*, **63**(6), 510-517. https://doi.org/10.1680/geot.11.P.088.

Cheng, Y., Yang, H.W. and Sun, D. (2018), "Cavity expansion in unsaturated soils of finite radial extent", *Comput. Geotech.*, **102**, 216-228. https://doi.org/10.1016/j.compgeo.2018.06.013.

Collins, I.F., Pender, M.J. and Yan, W. (1992), "Cavity expansion in sands under drained loading conditions", *Int. J. Numer. Anal. Meth. Geomech.*, **16**(1), 3-23. https://doi.org/10.1016/0148-9062(92)92891-F.

Collins, I.F. and Stimpson, J.R. (1994), "Similarity solutions for drained a undrained cavity expansions in soils", *Geotechnique*, **44**(1), 21-34. https://doi.org/10.1680/geot.1994.44.1.21.

Davis, E.H. (1969), *Chapter six: Theories of Plasticity and the Failure of Soil Masses*, (Ed., I.K. Lee), Butterworths, London, England.

Fredlund, D.G. and Xing, A. (1994), "Equations for the soil-water characteristic curve", *Can. Geotech. J.*, **31**(4), 521-532. https://doi.org/10.1139/t94-061.

Futai, M.M., Almeida, M.S.S. and Lacerda, W.A. (2004), "Yield, strength, and critical state behavior of a tropical saturated soil", *J. Geotech. Geoenviron. Eng.*, **130**(11), 1169-1179. https://doi.org/10.1061/(asce)1090-0241(2004)130:11(1169).

Khalili, N., Habte, M.A. and Zargarbashi, S. (2008), "A fully coupled flow deformation model for cyclic analysis of unsaturated soils including hydraulic and mechanical hysteresis", *Comput. Geotech.*, **35**(6), 872-889. https://doi.org/10.1016/j.compgeo.2008.08.003.

Latib, F.W.M., Taha, M.R. and Kasa, A. (2018), "A review on critical state parameters of residual soil", *J. Eng. Appl. Sci.*, **13**(17), 7465-7470. https://doi.org/10.36478/jeasci.2018.7465.7470.

Lee, S.W., Kim, T.S., Sim, B.K., Kim, J.S. and Lee, I.M. (2012), "Effect of pressurized grouting on pullout resistance and group efficiency of compression ground anchor", *Can. Geotech. J.*, **49**(8), 939-953. https://doi.org/10.1139/t2012-059.

Li, C. and Zou, J.F. (2019), "Created cavity expansion solution in anisotropic and drained condition based on Cam-Clay model", *Geomech. Eng.*, **19**(2), 141-151. https://doi.org/10.12989/gae.2019.19.2.141.

Li, C., Zou, J.F. and A.S. (2019a), "Closed-form solution for undrained cavity expansion in anisotropic soil mass based on spatially mobilized plane failure criterion", *Int. J. Geomech.*, **19**(7), 04019075. https://doi.org/10.1061/(asce)gm.1943-5622.0001458.

Li, C., Zou, J.F. and Li, L. (2019b), "Elasto-plastic solution for cavity expansion problem in anisotropic and drained soil mass", *Geomech. Eng.*, **19**(6), 513-522. https://doi.org/10.12989/gae.2019.19.6.513.

Li, C., Zou, J.F. and Sheng, Y.M. (2020), "Undrained solution for cavity expansion in strength degradation and tresca soils", *Geomech. Eng.*, **21**(6), 527-536. https://doi.org/10.12989/gae.2020.21.6.527.

Li, L., Xiang, Z.C., Zou, J.F. and Wang, F. (2019c), "An improved model of compaction grouting considering three-dimensional shearing failure and its engineering application", *Geomech. Eng.*, **19**(3), 217-227. https://doi.org/10.12989/gae.2019.19.3.217.

Lu, N. and Kaya, M. (2014), "Power law for elastic moduli of unsaturated soil", *J. Geotech. Geoenviron. Eng.*, **140**(1), 46-56. https://doi.org/10.1061/(asce)gt.1943-5606.0000990.

Ng, C.W.W., Xu, J. and Yung, S.Y. (2009), "Effects of wetting–drying and stress ratio on anisotropic stiffness of an unsaturated soil at very small strains", *Can. Geotech. J.*, **46**(9), 1062-1076. https://doi.org/10.1139/t09-043.

Rouainia, M., Panayides, S., Arroyo, M. and Gens, A. (2020), "A pressuremeter-based evaluation of structure in london clay using a kinematic hardening constitutive model", *Acta Geotech.*, **15**(8), 2089-2101. https://doi.org/10.1007/s11440-020-00940-w.

Russell, A.R. (2014), "How water retention in fractal soils depends on particle and pore sizes, shapes, volumes and surface areas", *Géotechnique*, **64**(5), 379-390. https://doi.org/10.1680/geot.13.p.165.

Russell, A.R. and Buzzi, O. (2012), "A fractal basis for soil-water characteristics curves with hydraulic hysteresis", *Geotechnique*, **62**(3), 269-274. https://doi.org/10.1680/geot.10.p.119.

Russell, A.R. and Khalili, N. (2006), "On the problem of cavity expansion in unsaturated soils", *Comput. Mech.*, **37**(4), 311-330. https://doi.org/10.1007/s00466-005-0672-7.

Salgado, R. and Prezzi, M. (2007), "Computation of cavity expansion pressure and penetration resistance in sands", *Int. J. Geomech.*, **7**(4), 251-265. https://doi.org/10.1061/(asce)1532-3641(2007)7:4(251).

Salgado, R. and Randolph, M.F. (2001), "Analysis of cavity expansion in sand", *Int. J. Geomech.*, **1**(2), 175–192. https://doi.org/10.1061/(asce)1532-3641(2001)1:2(175).

Schanz, T. and Vermeer, P.A. (1996), "Angles of friction and dilatancy of sand", *Geotechnique*, **46**(1), 145-151. https://doi.org/10.1680/geot.1996.46.1.145.

Schnaid, F., Kratz de Oliveira, L.A. and Gehling, W.Y.Y. (2004), "Unsaturated constitutive surfaces from pressuremeter tests", *J. Geotech. Geoenviron. Eng.*, **130**(2), 174-185. https://doi.org/10.1061/(asce)1090-0241(2004)130:2(174).

Schnaid, F., Ortigao, J.A., Mántaras, F.M., Cunha, R.P. and MacGregor, I. (2000), "Analysis of self-boring pressuremeter (SBPM) and Marchetti dilatometer (DMT) tests in granite saprolites", *Can. Geotech. J.*, **37**(4), 796-810. https://doi.org/10.1139/t00-005.

Tang, J., Wang, H. and Li, J. (2021), "A semi-analytical solution to spherical cavity expansion in unsaturated soils", *Geomech. Eng.*, **25**(4), 283-294. https://doi.org/10.12989/gae.2021.25.4.283.

Thiyyakkandi, S., McVay, M., Bloomquist, D. and Lai, P. (2013), "Measured and predicted response of a new jetted and grouted precast pile with membranes in cohesionless soils", *J. Geotech. Geoenviron. Eng.*, **139**(8), 1334-1345. https://doi.org/10.1061/(asce)gt.1943-5606.0000860.

Wang, Y., Li, L. and Li, J. (2021), "A similarity solution for undrained expansion of a cylindrical cavity in K_0-consolidated anisotropic soils", *Geomech. Eng.*, **25**(4), 303-315. https://doi.org/10.12989/gae.2021.25.4.303.

Yang, H. and Russell, A.R. (2015a), "Cavity expansion in unsaturated soils exhibiting hydraulic hysteresis considering three drainage conditions", *Int. J. Numer. Anal. Meth. Geomech.*, **39**(18), 1975-2016. https://doi.org/10.1002/nag.2379.

Yang, H. and Russell, A.R. (2015b), "Cone penetration tests in unsaturated silty sands", *Can. Geotech. J.*, **53**(3), 431-444.

https://doi.org/10.1139/cgj-2015-0142.

Yu, H.S. and Carter, J.P. (2002), "Rigorous similarity solutions for cavity expansion in cohesive-frictional soils", *Int. J. Geomech.*, **2**(2), 233-258. https://doi.org/10.1061/(asce)1532-3641(2002)2:2(233).

Yu, H.S. and Houlsby, G.T. (1991), "Finite cavity expansion in dilatant soils: loading analysis", *Geotechnique*, **41**(2), 173-183. https://doi.org/10.1680/geot.1991.41.2.173.

Zhang, J. and Salgado, R. (2010), "Stress–dilatancy relation for mohr–coulomb soils following a non-associated flow rule", *Géotechnique*, **60**(3), 223-226. https://doi.org/10.1680/geot.8.t.039.

Zhao, C.F., Fei, Y., Zhao, C. and Jia, S.H. (2018), "Analysis of expanded radius and internal expanding pressure for undrained cylindrical cavity expansion", *Int. J. Geomech.*, **18**(2), 04017139. https://doi.org/10.1061/(asce)gm.1943-5622.0001058.

GC